Atom Indonesia

Journal homepage: http://aij.batan.go.id

Synthesis and Characterization of Stoichiometric Spinel-$LiMn_2O_4$

T.Y.S. Panca Putra[1*], Deswita[1], A. Insani[1], H. Mugiraharjo[1], E. Sukirman[1], A.K. Jahja[1], T.H. Priyanto[1], S. Lee[2] and T. Kamiyama[3]

[1]*Center for Science and Technology of Advanced Materials, National Nuclear Energy Agency, Kawasan Puspiptek Serpong, Tangerang Selatan 15314, Indonesia*

[2]*High-Flux Advanced Neutron Application Reactor, Korea Atomic Energy Research Institute (KAERI), 150-1 Deokjin-Dong, 1045 Daedeokdaero, Yuseong-gu, Daejeon 305-600, Korea*

[3]*High Energy Accelerator Research Organization, 1-1 Oho, Tsukuba, Ibaraki 305-0801, Japan*

ARTICLE INFO

Article history:
Received 29 October 2016
Received in revised form 6 November 2017
Accepted 9 November 2017

Keywords:
Stoichiometric
$LiMn_2O_4$
Phase transition
Structure

ABSTRACT

In this study, spinel $LiMn_2O_4$ powder was synthesized from $LiOH.H_2O$ and MnO_x by conventional and mechanical alloying (MA) methods, followed by heat treatment at 800 °C in O_2 for four hours with cooling to room temperature in the furnace at 60 °C/h. It is found that both samples do not show phase transition in low temperature, and this occurred for different reasons. In the MA sample, the presence of Fe as contamination increased the Mn valence and hindered the occurrence of phase transition. The conventional sample does not show phase transition at low temperature due to stoichiometric content, without any contamination. In general, the absence of phase transition occurred due to synthesis condition employed in this study.

INTRODUCTION*

Spinel $LiMn_2O_4$ has attracted attention, both in terms of its structure and its application, in an effort to find a suitable material for the cathode in an Li-ion battery system. On the other hand, it is accepted in general that the physical and electrochemical properties of $LiMn_2O_4$ are determined by such factors as particle size, lattice parameter, stoichiometry, average Mn valence, surface morphology, and homogeneity [1-5]. In practice, these factors are closely related to the synthesis method and condition, such as starting material, content of lithium, heating temperature, holding time, and cooling rate [6-12].

It is important to ensure that $LiMn_2O_4$ contains a sufficient amount of Mn^{4+} and a low content of Mn^{3+} in order to maintain average Mn valence above 3.5^+. Lower average Mn valences will cause Jahn-Teller distortion during electrochemical processes and lead to capacity fading of spinel $LiMn_2O_4$ [13]. The spinel $LiMn_2O_4$ has an average Mn valence of 3.5^+, which is just a critical point, and will easily be interfered even by a slight change in synthesis condition, due to charge compensation. Previous works suggested some factors responsible for a phase transition in spinel $LiMn_2O_4$, such as partial charge ordering of Mn^{3+} and Mn^{4+} [12] and Jahn-Teller distortion [14]. A report showed that the absence of Jahn-Teller ordering is related to stoichiometric spinel without phase transition at low temperature [15]. Another result showed that the phase transition is closely related to the population of oxygen vacancies and its presence is the sole and necessary condition for the phase transition, not the synthesis temperature or the thermal treatment history [16].

It was proposed that in a strictly stoichiometric sample, this phase transition should not occur. In order to obtain a strictly stoichiometric $LiMn_2O_4$, a synthesis method should be selected carefully while the synthesis condition should be controlled simultaneously. Mechanical alloying (MA) and conventional mixing method in a mortar are common among many methods used to synthesize $LiMn_2O_4$, and previous works showed various results of $LiMn_2O_4$ synthesis. In this paper, the use of both methods is reported and the

*Corresponding author.
E-mail address: teguhpanca@batan.go.id
DOI: https://doi.org/10.17146/aij.2017.542

relationship among the synthesis condition, the physical properties, and the stoichiometry of the spinel $LiMn_2O_4$ are described. In particular, the stoichiometry of the synthesized $LiMn_2O_4$ and the structure were determined in relation to the occurrence of phase transition. Characterizations were carried out by several methods, namely by scanning electron microscope (SEM), thermogravimetry-differential thermal analysis (TG-DTA), and X-ray diffraction (XRD). In order to accurately determine the site occupancies of light atoms such as lithium, or even oxygen, in the presence of manganese, and also to clarify structural details of spinel $LiMn_2O_4$, neutron powder diffraction (NPD) was employed [13]. NPD is a powerful and suitable means for structural determination because of the difference in the coherent scattering lengths of atoms in $LiMn_2O_4$.

EXPERIMENTAL METHODS

Synthesis of spinel-$LiMn_2O_4$

Spinel $LiMn_2O_4$ was synthesized from starting materials of $LiOH{\cdot}H_2O$ as lithium sources and MnO_x obtained by thermal decomposition of manganese oxalate. Stoichiometric amounts of $LiOH{\cdot}H_2O$ and MnO_x were charged into a stainless steel jar with an internal volume of 125 mL in molar ratio of Li/Mn=0.50. Mechanical alloying (MA) was carried out using a planetary ball mill (Retsch PM 200) and stainless steel balls (10 mm diameter) with various parameters. The weight ratio of balls and materials was 40:1. The rotation speed of the miller was 500 rpm. Spinel $LiMn_2O_4$ was also synthesized by conventional mixing of starting materials in a mortar for comparison. The mixtures were then pressed into pellets and heated at 800 °C in O_2 for four hours with cooling to room temperature in the furnace at 60 °C/h.

Characterization of spinel-$LiMn_2O_4$

The morphology of the spinel was analyzed using the JEOL JSM-6510LA SEM at PSTBM-BATAN, Indonesia. Thermal analysis was conducted with a Setaram TAG-24S DTA/TG at Ibaraki University, Japan, using alumina crucible, in argon. The rate of heating was 10 °C/min. The structure of the as-prepared powders was studied by X-ray diffraction (Rigaku Ultima IV XRD) at Rigaku, Japan, using Cu Kα radiation at the temperature range of 20 °C to -180 °C. The lattice parameter of prepared spinel phases was analyzed by built-in software package PDXL with Si as reference. Neutron diffraction data were measured at the neutron HRPD of HANARO-KAERI, South Korea (λ = 1.83433 Å) at 15 K, 150 K, and 300 K, while neutron diffraction data of standard $LiMn_2O_4$ measured at 300 K were obtained from HRPD of BATAN, Indonesia (λ = 1.82230 Å). The structural parameters were refined with FullProf for the data from HANARO-KAERI and by Z-Rietveld [17,18] for the data from HRPD-BATAN.

RESULTS AND DISCUSSION

Figures 1(a) and 1(b) show the morphology of spinel samples synthesized from $LiOH.H_2O$ and MnO_x obtained by MA for six hours and conventional method, then annealed at 800 °C for four hours in O_2 and cooled down to room temperature with cooling rate 60 °C/h. The two samples seem to show similar morphologies with distinctive individual granules whose size is about several hundreds nanometers and some aggregation. In general, the annealing process with the same conditions for both samples caused the particles growth and aggregation of smaller particles regardless of the initial mixing methods.

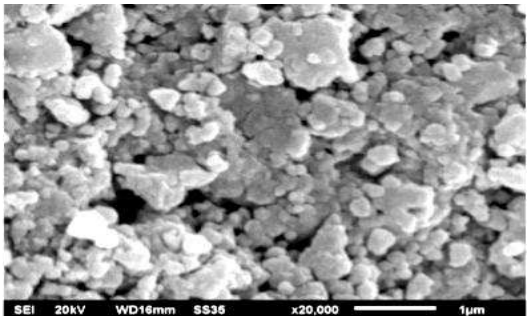

(a)

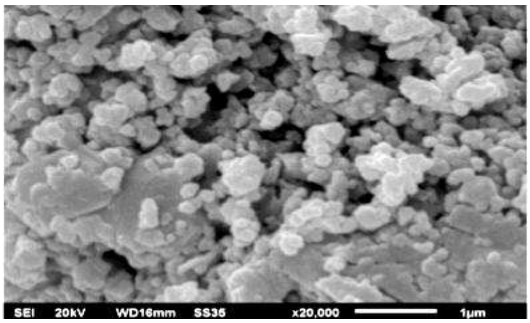

(b)

Fig. 1. SEM micrograph of the spinel-type $LiMn_2O_4$ synthesized with an initial molar ratio of Li/Mn = 0.50 (a) after MA for 6 hours and (b) conventionally prepared, and after annealed at 800 °C for 4 hours in O_2 then cooled with cooling rate of 60 °C/h.

Figure 2 shows TG profiles and DTA curves of Li-Mn-O mixtures synthesized by MA for six hours and by conventional method, then annealed at 800 °C for four hours in O_2 and cooled down

to room temperature with cooling rate 60 °C/h. The DTA curves of both samples show similar patterns. The related TG profile of both samples shows that the mass changed gradually until around 700 °C and then declined sharply until 900 °C. The common value of mass loss in MA sample is lower than in the conventional sample at all temperatures. Therefore, it serves as evidence that the MA sample has a better thermal stability than conventional sample because the mixing of raw materials during MA was more controlled throughout the process, which leads to a consistent contact and reaction between raw materials powder. Above 800 °C, both samples show mass losses and are related to the decomposition process of $LiMn_2O_4$.

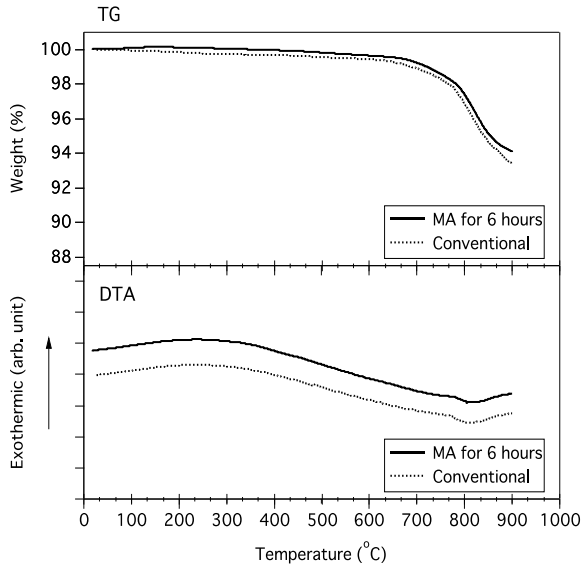

Fig. 2. TG-profiles and DTA-curves of the mixture of $LiOH.H_2O$ and MnO_x with an initial molar ratio of Li/Mn = 0.50 synthesized by MA for 6 hours and conventional method and subsequent annealing at 800 °C for 4 hours in O_2 with cooling rate of 60 °C/h.

Figure 3 shows the XRD patterns of the spinel $LiMn_2O_4$ synthesized from $LiOH.H_2O$ and MnO_x by conventional and MA methods, measured at temperature range from room temperature down to 93K. Previous works [19,20] showed that at room temperature, stoichiometric spinel oxide, $LiMn_2O_4$, display a cubic, normal spinel structure (space group *Fd-3m*). The transformation should start at near room temperature (~290 K) and is shown by peak splitting of the spinel diffraction lines with decreasing temperature. The diffraction patterns from the samples synthesized from $LiOH.H_2O$ and MnO_x by conventional and MA methods in this study, however, did not show any significant changes such as peak splitting down to 93 K, as shown in Figs. 3(b) and (d).

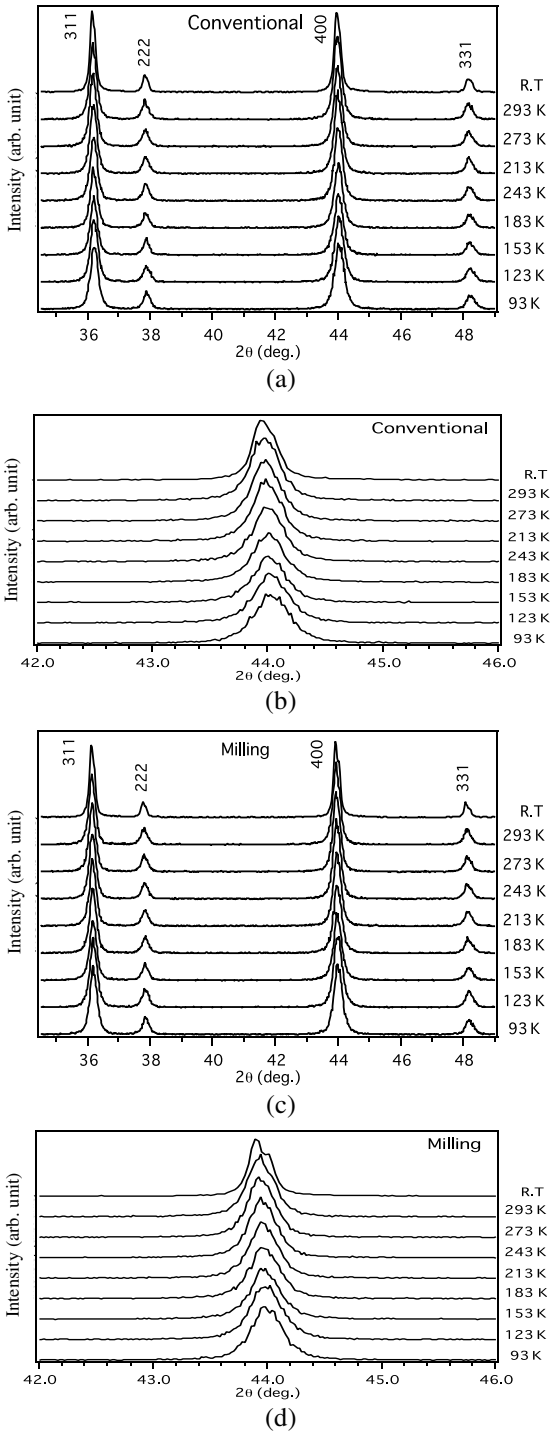

Fig. 3. XRD patterns of the spinel-type $LiMn_2O_4$ synthesized with an initial molar ratio of Li/Mn = 0.50 by conventional method (a) and (b) and MA method for 6 hours (c) and (d) and annealed at 800 °C for 4 hours in O_2 then cooled with cooling rate of 60 °C/h. (a) and (c) 2θ region from 34.5 ° to 49 ° and (b) and (d) peaks of (400) plane.

In Fig. 4(a), however, it is revealed that lattice constant *a* increased with temperature. Peak broadenings, shown as FWHM in Fig. 4(b), are observed for all reflections and getting larger as measurement temperature decreased. It is notable that peak broadening was larger and lattice constant *a* was smaller for conventional mixing sample

compared with MA sample. The result indicates that phase transition at low temperatures was not obvious for these samples.

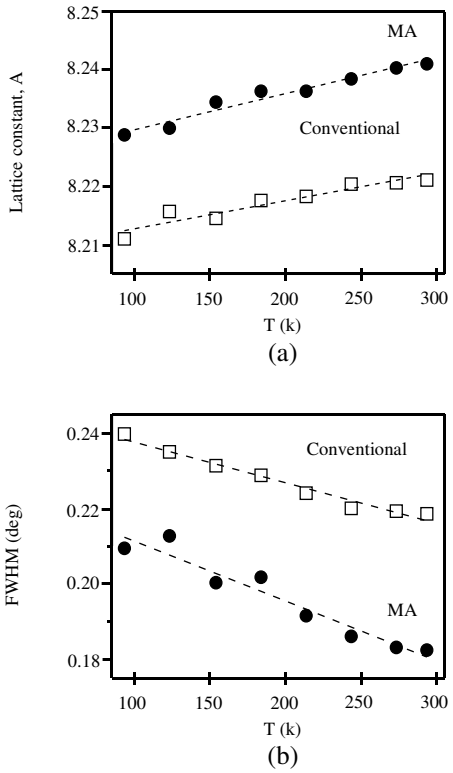

Fig. 4. (a) lattice constant *a* of the cubic $LiMn_2O_4$ and (b) Gaussian FWHM, plotted as a function of measuring temperature. The data were obtained by XRD measurements.

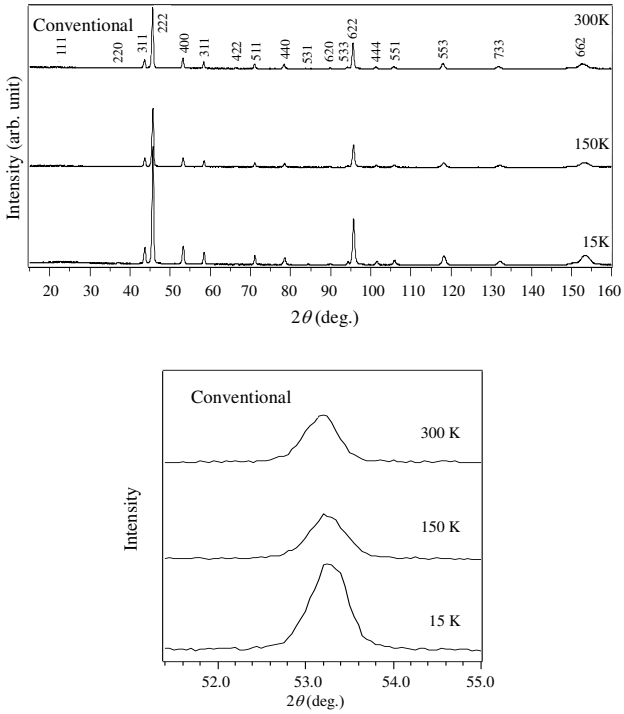

Fig. 5. Neutron diffraction patterns taken from HRPD-HANARO of the spinel-type $LiMn_2O_4$ synthesized with an initial molar ratio of Li/Mn = 0.50 by conventional method and annealed at 800 °C for 4 hours in O_2 then cooled with cooling rate of 60 °C/h. (a) whole pattern and (b) (400) peaks.

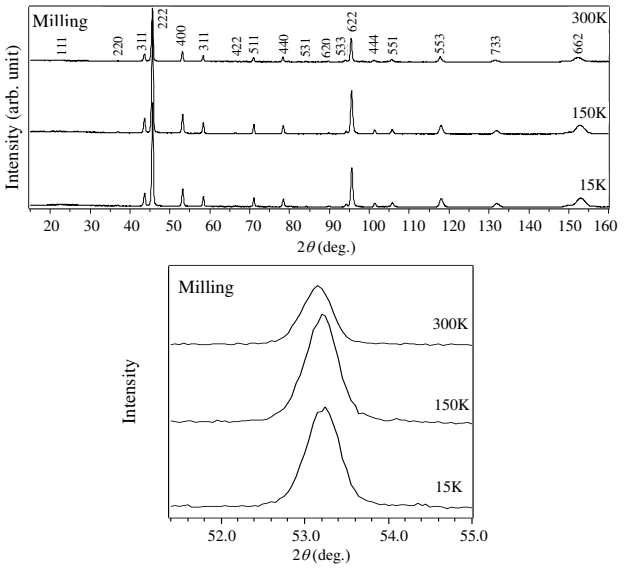

Fig. 6. Neutron diffraction patterns taken from HRPD-HANARO of the spinel-type $LiMn_2O_4$ synthesized with an initial molar ratio of Li/Mn = 0.50 by MA method and annealed at 800 °C for 4 hours in O_2 then cooled with cooling rate of 60 °C/h. (a) whole pattern and (b) (400) peaks.

Figures 5 and 6 show the neutron diffraction obtained with HRPD-HANARO of the spinel $LiMn_2O_4$ synthesized by MA and conventional methods, respectively, after measurements at temperatures of 300 K, 150 K, and 15 K. The patterns do not show any peak splitting, which is consistent with the result from XRD. Figures 7(a) and 7(b) show the profile fitting of neutron diffraction data.

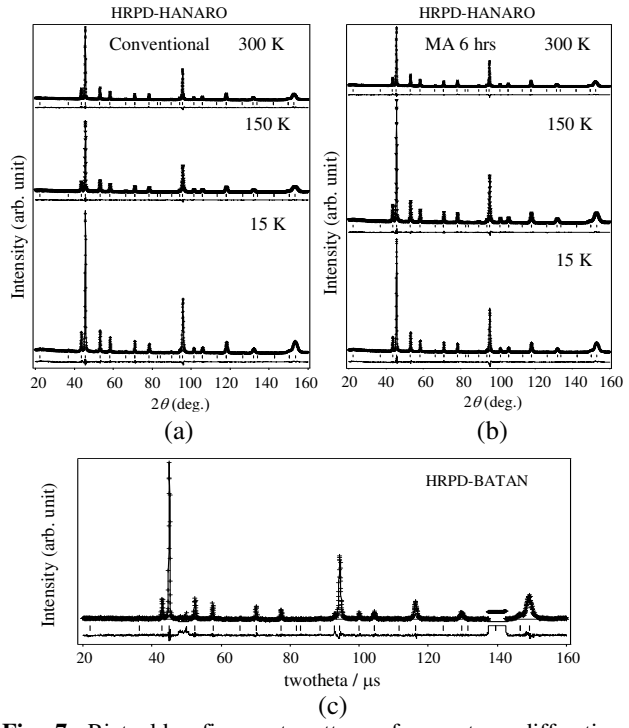

Fig. 7. Rietveld refinement patterns for neutron diffraction measurement at 15K, 150K and 300K (HRPD-HANARO) of spinel $LiMn_2O_4$ synthesized by a) conventional and b) MA methods and annealed at 800 °C in O_2. (c) commercial/standard $LiMn_2O_4$ measured at 300K (HRPD-BATAN).

Table 1. Refined structure parameters of spinel-$LiMn_2O_4$.

			Temperature of measurement/K					
			15		150		300	
Synthesis Method			MA	Conv.	MA	Conv.	MA	Conv.
Lattice Parameter/Å		*a*	8.22337(72)	8.21622(71)	8.22650(63)	8.22000(83)	8.23488(69)	8.22880(70)
Atomic Coordinates								
	Li(1)	*g*	0.97271	1	0.97271	1	0.97271	1
		x	1/8	1/8	1/8	1/8	1/8	1/8
		B/Å^2	0	0	0	0	0	0
	Mn(1)	*g*	0.96269	1	0.96269	1	0.96269	1
		x	1/2	1/2	1/2	1/2	1/2	1/2
		B/Å^2	0	0	0	0	0	0
	O(1)	*g*	1	1	1	1	1	1
		x	0.26320(7)	0.26307(7)	0.26271(6)	0.26281(8)	0.26307(7)	0.26296(7)
		B/Å^2	0	0	0	0	0	0
	Fe	*g*	0.01392	-	0.01392	-	0.01392	-
		x	1/2	-	1/2	-	1/2	-
		B/Å^2	0	-	0	-	0	-
	Cr	*g*	0.00243	-	0.00243	-	0.00243	-
		x	1/2	-	1/2	-	1/2	-
		B/Å^2	0	-	0	-	0	-
R-Factors		*S*	1.68	1.51	1.48	1.19	1.15	1.09
		R_{wp}/ %	14.6	14.3	12.5	16.0	14.1	14.7
		R_e/ %	8.67	9.44	12.7	13.4	12.2	13.5

Note:
Li(1) is located at 8*a* site with coordinates (1/8, 1/8, 1/8); Mn(1) is located at 16*d* site with coordinates (1/2, 1/2, 1/2); O(1) is located at 32*e* site with coordinates (*x*, *x*, *x*).
Space group: *Fd-3m* (No. 227, origin choice 2).

Table 2. Anisotropic temperature factors (Å^2) of spinel-$LiMn_2O_4$.

			Temperature of measurement/K					
			15		150		300	
Synthesis Method			MA	Conv.	MA	Conv.	MA	Conv.
Li(1)	B_{11}	0.0113(7)	0.0135(7)	0.0123(6)	0.0145(9)	0.0135(7)	0.0132(7)	
	B_{22}	= B_{11}(Li1)	= B_{11}(Li1)	= B_{11}(Li1)	= B_{11}(Li1)	= B_{11}(Li1)	= B_{11}(Li1)	
	B_{33}	= B_{11}(Li1)	= B_{11}(Li1)	= B_{11}(Li1)	= B_{11}(Li1)	= B_{11}(Li1)	= B_{11}(Li1)	
	B_{12}	0	0	0	0	0	0	
	B_{13}	0	0	0	0	0	0	
	B_{23}	0	0	0	0	0	0	
Mn(1)	B_{11}	0.0074(2)	0.0081(2)	0.0075(1)	0.0085(2)	0.0087(2)	0.0091(2)	
	B_{22}	= B_{11}(Mn1)	= B_{11}(Mn1)	= B_{11}(Mn1)	= B_{11}(Mn1)	= B_{11}(Mn1)	= B_{11}(Mn1)	
	B_{33}	= B_{11}(Mn1)	= B_{11}(Mn1)	= B_{11}(Mn1)	= B_{11}(Mn1)	= B_{11}(Mn1)	= B_{11}(Mn1)	
	B_{12}	-0.0003(2)	-0.0003(2)	-0.0002(2)	0.0000(2)	-0.0006(2)	0.0006(2)	
	B_{13}	= B_{12}(Mn1)	= B_{12}(Mn1)	= B_{12}(Mn1)	= B_{12}(Mn1)	= B_{12}(Mn1)	= B_{12}(Mn1)	
	B_{23}	= B_{12}(Mn1)	= B_{12}(Mn1)	= B_{12}(Mn1)	= B_{12}(Mn1)	= B_{12}(Mn1)	= B_{12}(Mn1)	
O(1)	B_{11}	0.0087(1)	0.0088(1)	0.0092(1)	0.0094(1)	0.0101(1)	0.0095(1)	
	B_{22}	= B_{11}(O1)	= B_{11}(O1)	= B_{11}(O1)	= B_{11}(O1)	= B_{11}(O1)	= B_{11}(O1)	
	B_{33}	= B_{11}(O1)	= B_{11}(O1)	= B_{11}(O1)	= B_{11}(O1)	= B_{11}(O1)	= B_{11}(O1)	
	B_{12}	- 0.00003(11)	-0.00002(12)	-0.0001(1)	-0.0001(1)	-0.0004(1)	-0.0002(1)	
	B_{13}	= B_{12}(O1)	= B_{11}(O1)	= B_{12}(O1)	= B_{11}(O1)	= B_{12}(O1)	= B_{11}(O1)	
	B_{23}	= B_{12}(O1)	= B_{11}(O1)	= B_{12}(O1)	= B_{11}(O1)	= B_{12}(O1)	= B_{11}(O1)	

The refinement fitted the adapted cubic *Fd-3m* symmetry. A comparison was made between the synthesized and standard $LiMn_2O_4$, as shown in Fig. 7(c) of neutron diffraction pattern taken from HRPD-BATAN. The two samples show similar patterns without any peak splitting. The synthesized $LiMn_2O_4$ had lattice constant *a* of 8.23488(69) Å (for MA) and 8.22880(70) Å (for conventional) at 300 K, comparable to 8.23668(19) Å of standard $LiMn_2O_4$. This result leads to a conclusion that synthesized samples were stoichiometric.

There was a decrease in lattice constant *a* with decreasing measurement temperature as summarized in Tables 1 and 2 and depicted in Fig. 8. As can be seen in this figure, the Li–O and Mn–O distances decreased with decreasing measurement temperature. During the refinement of conventional samples, the occupancies of oxygen at all measurement temperatures were found to be greater than one, indicating no observable oxygen deficiency and all samples being stoichiometric.

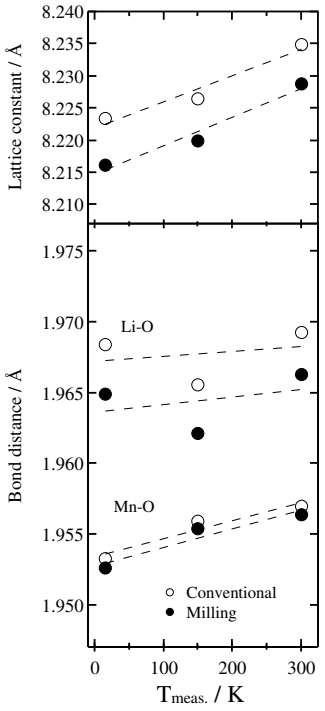

Fig. 8. Bond distances (Li–O, Mn–O) of the spinel-type $LiMn_2O_4$ as a function of measurement temperature.

The refinement for MA samples by using stainless steel jar and balls also considered the Fe and Cr contents from chemical analysis by ICP-AAS [16]. The result shows fully occupied oxygen as well. The absence of a phase transition in both samples occurred due for different reasons. The samples synthesized by using stainless steel jar and balls contained Fe, resulting in occupancy of Fe at Mn site (16*d*), and eventually increasing Mn oxidation state and hindering the occurrence of a phase transition. The result from data refinement shows that the oxygen sites were fully occupied. It was therefore concluded that the absence of a phase transition is closely related to the synthesis condition employed in this study such as: the moderate synthesis temperature (800 °C), the use of O_2 atmosphere to induce more oxidative reaction, the slow cooling rate (60 °C/h), and the use of more reactive starting materials ($LiOH.H_2O$ and MnO_x).

CONCLUSION

Spinel $LiMn_2O_4$ powder has been synthesized by MA and conventional method. It was found that in the MA sample produced by using stainless steel jar and balls, the presence of Fe as contamination, situated at Mn site (16*d*), increased the Mn valence and hindered the occurrence of a phase transition. The conventional samples synthesized from reactive starting material, *i.e.* $LiOH.H_2O$ and MnO_x, and annealed at 800 °C in O_2 with slow cooling rate did not show a phase transition at low temperature.

The phase transition in spinel $LiMn_2O_4$ at low temperature as an indication of non-stoichiometric $LiMn_2O_4$ did not occur in studies by means of XRD and neutron powder diffraction (NPD). Generally, the absence of a phase transition was due to synthesis conditions employed in this study such as: the moderate synthesis temperature (800 °C), the use of O_2 atmosphere to induce more oxidative reaction, the slow cooling rate (60 °C/h), and the use of more reactive starting materials ($LiOH.H_2O$ and MnO_x). It is concluded that stoichiometric spinel without any contamination was successfully obtained by conventional method.

ACKNOWLEDGMENT

T.Y.S.P.P. is grateful for all support kindly provided by BATAN, Indonesia, KAERI, South Korea, and MEXT, Japan. The neutron diffraction experiment was supported by the S-type project of KEK with the proposal No. 2009S05 and is greatly acknowledged. Valuable discussion and suggestion from the members of Powder Diffraction Group in BATAN, KEK, and J-PARC, from the members of Kanno and Hirayama's Lab, and from Prof. T. Sakuma of Ibaraki University are greatly acknowledged.

REFERENCES

1. J. Lu, C. Zhou, Z. Liu *et al.*, Electrochim. Acta **212** (2016) 553.
2. A. Swiderska-Mocek and D. Naparstek, Solid State Ionics **267** (2014) 32.
3. J.P. Silva, S.R. Biaggion, N. Bocchi *et al.*, Solid State Ionics **268** (2014) 42.

4. A. Mukhopadhyay and B.W. Sheldon, Prog. Mater. Sci. **63** (2014) 58.
5. A. Tron, Y.D. Park and J. Mun, J. Power Sources **325** (2016) 360.
6. D. Zhan, F. Yang, Q. Zhang *et al.*, Electrochim. Acta **129** (2014) 364.
7. X.-W. Liu, J. Tang, X.-S. Qin *et al.*, Transactions of Nonferrous Metals Society of China **24** (2014) 1414.
8. S. Zhao, Q. Chang, K. Jiang *et al.*, Solid State Ionics **253** (2013) 1.
9. C.-L. Chen, K.-F. Chiu, Y.-R. Chen *et al.*, Thin Solid Films **544** (2013) 182.
10. D.-L. Fang, J.-C. Li, X. Liu *et al.*, J. Alloys Compd. **640** (2015) 82.
11. Y. Cai, Y. Huang, X. Wang *et al.*, Ceram. Int. **40** (2014) 14039.
12. D. Zhan, Q. Zhang, X. Hu *et al.*, Solid State Ionics **239** (2013) 8.
13. T.Y.S. Panca Putra, M. Yonemura, S. Torii *et al.*, Solid State Ionics **262** (2014) 83.
14. N. West, K.I. Ozoemena, C.O. Ikpo *et al.*, Electrochim. Acta **101** (2013) 86.
15. R. Kanno, M. Yonemura, T. Kohigashi *et al.*, J. Power Sources **97-98** (2001) 423.
16. X.Q. Yang, X. Sun, M. Balasubramanian *et al.*, Electrochem. Solid-State Lett. **4** (2001) A117.
17. R. Oishi, M. Yonemura, Y. Nishimaki *et al.*, Nucl. Instrum. Methods Phys. Res. **A 600** (2009) 94.
18. R. Oishi-Tomiyasu, M. Yonemura, T. Morishima *et al.*, J. Appl. Cryst. **45** (2012) 299.
19. S. Bagˇcı, H.M. Tütüncü, S. Duman *et al.*, J. Phys. Chem. Solids **75** (2014) 463.
20. P. Piszora, W. Paszkowicz, C. Baehtz *et al.*, J. Alloys Compd. **382** (2004) 119.